Structural Durability & Health Monitoring

Tech Science Press

https://doi.org/10.32604/sdhm.2026.075835

ARTICLE

# Research on Mechanical Properties of the Composite Bridge Deck System Composed of Orthotropic Steel Deck and RPC Layer under Normal Temperature Curing

**Hui Zhang[1,*], Yingying Xie[1], Yu Zhang[2,*], Zhan Gao[1], Aijun Li[1], Sheng Shi[1], Xingyue Li[1], Zheming Zhou[1] and Haotian Wang[1]**

[1]School of Civil Engineering, Lanzhou Jiaotong University, Lanzhou, China
[2]School of Traffic and Transportation, Lanzhou Jiaotong University, Lanzhou, China

*Corresponding Authors: Hui Zhang. Email: 17352150551@163.com; Yu Zhang. Email: zhangyu@mail.lzjtu.cn

Received: 09 November 2025; Accepted: 15 January 2026; Published: 18 May 2026

**Featured Application:** The normal-temperature-cured RPC composite deck system presented in this study provides a practical and energy-efficient solution for the maintenance and reinforcement of orthotropic steel bridge decks. It enables engineers to significantly enhance the deck's durability and fatigue resistance against traffic loads without the need for complex, high-temperature curing processes on site. This technology is particularly promising for extending the service life of existing bridges and for constructing more resilient new bridges with reduced environmental impact and lifecycle costs.

**ABSTRACT:** A composite bridge deck system consisting of an orthotropic steel deck and a normal-temperature-cured reactive powder concrete (RPC) layer is proposed to address the problems of pavement damage and fatigue cracks in steel bridge decks. In this study, a local finite element model of a bridge segment was established using ANSYS to calculate and compare the stress states of four deck systems: normal-temperature-cured RPC composite box girders, high-temperature-cured RPC composite box girders, pure steel box girders, and ordinary concrete composite box girders. Additionally, static load tests were conducted on a scaled local model to validate the finite element results. The results show that the compressive strength, flexural strength, and elastic modulus of the normal-temperature-cured RPC are significantly improved compared with those of ordinary concrete. The maximum tensile stress in the normal-temperature-cured RPC layer reached 6.45 MPa without cracking, which is much higher than the tensile capacity of ordinary concrete, thereby offering a solution to pavement failure. The stress in the steel deck was reduced by more than 80% for both normal- and high-temperature-cured RPC composite decks, which is significantly greater than the reduction achieved by the ordinary concrete composite deck. This substantial stress reduction greatly enhances the fatigue life of the bridge deck. Therefore, the RPC composite deck system can effectively improve the fatigue performance of orthotropic steel bridge decks.

**KEYWORDS:** Orthotropic steel deck; normal temperature maintenance; reactive powder concrete

## 1 Introduction

Modern bridge engineering widely employs long-span lightweight steel box girders with orthotropic steel decks (OSDs) due to their exceptional high strength-to-weight ratio [1]. However, the long-term service performance of OSDs is often constrained by two interrelated typical damage modes: accelerated deterioration of the deck pavement and fatigue cracking in the underlying steel plate [2–4]. These issues

not only lead to frequent and costly repairs but also undermine the structural resilience of the bridge system—that is, its capacity to withstand, adapt to, and recover from damage [5]. Fatigue assessments based on field monitoring and dynamic response further confirm the severity of this problem. Under heavy traffic conditions, the predicted fatigue life of critical structural details often fails to meet design expectations [6,7], a concern particularly pronounced in heavy-haul railway environments where dynamic effects are significant [8].

The root causes of these problems stem primarily from the inherent limitations of conventional paving systems. On one hand, conventional asphalt concrete pavement layers exhibit relatively low tensile strength and are prone to significant local stress concentrations under wheel loads, leading to premature cracking and raveling. On the other hand, due to their low elastic modulus and limited thickness, asphalt layers contribute negligibly to the overall stiffness of the OSD system. Consequently, the steel deck is continuously subjected to high stress amplitudes during long-term service, making it highly susceptible to fatigue cracking [9]. Existing research often addresses these two types of damage separately. For example, using modified paving materials such as epoxy asphalt concrete can enhance the durability of the surface layer [10], but their low stiffness provides limited improvement to the fatigue performance of the steel deck. Conversely, employing rigid overlays like steel fiber-reinforced concrete can significantly increase the overall structural stiffness [11,12], yet these materials often suffer from insufficient tensile resistance, leading to cracking within the overlay itself under repeated tensile stresses.

This contradiction reveals a critical technological gap: there is an urgent need for a paving solution that simultaneously possesses high stiffness (to reduce stress in the steel plate) and high tensile capacity (to ensure the integrity of the overlay). Ultra-High Performance Concrete (UHPC) and its derivative material—Reactive Powder Concrete (RPC)—are regarded as highly promising alternative materials due to their ultra-high strength, high elastic modulus, excellent durability, and toughness [13]. Engineering practice has shown that rehabilitating fatigued steel bridge decks with UHPC overlays can effectively reduce stress levels at critical details and significantly extend structural life [14,15]. However, the application of UHPC/RPC also faces a series of new challenges: these include complex stress transfer at the steel-UHPC interface and fatigue issues of shear connectors, the latter involving specialized analysis of stud shear strength and performance [15,16], the impact of stud degradation and arrangement [17], as well as the risk of shrinkage-induced cracking due to the material's high shrinkage and strong restraint, which may even require special construction techniques like "post-combination" to mitigate [18]. Concurrently, the academic community continues to explore ways to enhance its sustainability by incorporating industrial solid wastes and developing low-carbon formulations, including innovative uses of materials like graphite tailings powder to drive a low-carbon transformation [19–23].

**Recent Advances and Persistent Challenges in RPC/UHPC for Bridge Decks**

Recent studies have further advanced our understanding of RPC/UHPC composite systems. Research has focused on optimizing mix designs for improved performance under ambient conditions [24,25], monitoring and mitigating shrinkage effects [26], and analyzing the fatigue performance of shear connectors in composite decks [27,28]. Additionally, both field applications and experimental studies have demonstrated that UHPC overlays are effective in rehabilitating fatigued orthotropic steel decks by improving fatigue resistance and extending service life [29], while advanced monitoring techniques have been developed for fatigue assessment based on strain data [23]. Despite these advancements, a noticeable disconnect remains between high-performance RPC developed in laboratories and technical solutions suitable for practical on-site engineering applications. This is mainly reflected in: (a) existing research and engineering applications still heavily rely on energy-intensive high-temperature steam curing to achieve its superior properties [19,22,24–26]; (b) most studies still view pavement durability or steel deck fatigue problems

in isolation [10–12,30], lacking integrated solutions that can systematically coordinate multiple objectives such as overlay crack resistance, extension of steel deck fatigue life, control of shrinkage stress, and green, low-carbon production, while also overlooking practical material innovations geared towards on-site construction [18,20,27]. Furthermore, the low activation efficiency of components like quartz powder in RPC under ambient temperatures further restricts its performance development [28]. This leads to a core question that urgently requires in-depth exploration: Can RPC with sufficient performance be produced through normal-temperature curing processes, in a practical and field-implementable manner, to simultaneously solve the dual challenges of overlay damage and steel deck panel fatigue?

**Research Gap and Objectives**

To bridge this gap between laboratory-grade high-performance materials and field-applicable, sustainable construction solutions, this study proposes and systematically investigates a novel composite deck system: integrating an orthotropic steel deck with a normal-temperature-cured RPC overlay via shear connectors. The research is designed to address two critical limitations in current practice:

(1) **Process Shift:** Moving from energy-intensive high-temperature curing to a practical normal-temperature wet-curing method, significantly improving on-site construction adaptability and environmental friendliness. This approach is inspired by recent advances in ambient-cured cementitious systems [20,25,27] and aligns with the broader pursuit of sustainable construction materials [16].
(2) **System Integration:** Providing a holistic solution aimed at simultaneously ensuring high crack resistance of the overlay and fatigue resistance of the steel deck within a single system. This moves beyond the limitations of "treating symptoms in isolation" found in existing studies [9–11,27] and strives to reduce reliance on complex construction techniques by virtue of the material's own superior properties [17], while also considering fundamental interface mechanics informed by studies on stud behavior [16,26].

**Main Contributions**

The main contributions of this study are threefold:

(1) **Feasibility Demonstration of Field-Applicable RPC:** This study confirms that RPC with mechanical properties fully meeting the requirements for deck pavement can be produced using a normal-temperature wet-curing regime, thereby eliminating dependence on on-site steam curing and offering a more sustainable and practical alternative for bridge rehabilitation and new construction.
(2) **Development and Validation of an Integrated Composite System:** We propose and experimentally validate a novel composite structural design that synergistically addresses the dual problems of overlay cracking and steel deck fatigue. By combining orthotropic steel deck with a normal-temperature-cured RPC layer, the system provides a comprehensive solution that enhances both durability and fatigue performance.
(3) **Quantification of Performance Benefits and Practical Implications:** Through systematic comparative analysis using finite element modeling and experimental testing, we quantify the significant benefits of the normal-temperature-cured RPC composite deck in terms of stress reduction (over 90% in steel deck), stiffness enhancement, and crack resistance. These findings provide clear justification for engineering applications and contribute to the development of more resilient and sustainable bridge infrastructure.

The research results indicate that the normal-temperature-cured RPC composite deck system proposed in this paper can effectively and simultaneously mitigate the two main types of damage in OSDs. This system not only reduces maintenance needs by significantly extending the fatigue life of the steel deck and providing a highly durable wearing surface but also, due to its normal-temperature curing process characteristics, contributes to enhancing the whole-life-cycle sustainability and operational resilience of bridge engineering.

## 2 Materials and Methods

### *2.1 RPC Material Components*

(1) Cement

Cement strength grades are designated as 32.5, 32.5R, 42.5, 42.5R, 52.5, 52.5R, 62.5, and 62.5R.

(2) Quartz Sand

Compared to other ordinary sands, quartz sand has higher hardness, which can improve the overall performance of concrete. The particle size selected in this study is 40–60 mesh.

(3) Quartz Powder

Quartz powder, also known as silica powder, exhibits strong resistance to erosion in acidic media. Common specifications include 100, 150, 200, 325, 400, 600, 1500, and 2000 M. The particle size of quartz powder used in this study is 1000 mesh.

(4) Silica Fume

Silica fume forms a cementitious gel with water, effectively binding cement particles and enhancing the tensile and compressive strength of concrete.

(5) Fly Ash

Fly ash is a fine powder derived from the flue gas produced during coal combustion. It reduces the heat of hydration, improves the density and impermeability of RPC, thereby reducing the likelihood of cracking.

(6) Steel Fibers

The steel fiber content is typically controlled by volume, with a recommended range of 1.5% to 3.0% for general applications. For critical structural components, the dosage may be appropriately increased. In this study, copper-plated straight steel fibers with a length of 13 mm and a diameter of approximately 0.2 mm were used. To significantly enhance the tensile performance and toughness of the RPC—a property crucial for resisting cracking in the deck overlay—a fiber content of 3.7% by volume was adopted. This dosage exceeds the common range of 1.5%–3.0% cited for ordinary purposes [10], aiming to maximize post-cracking behavior and fatigue resistance in the demanding context of orthotropic deck systems, a strategy supported by prior research on high-performance concrete overlays [12,13].

### *2.2 RPC Mixing Procedure*

The RPC mixture was prepared using an HJW-60 forced single horizontal shaft concrete mixer operating at a speed of 45 r/min. Prior to mixing, the blades and inner walls of the mixer were rinsed with clean water and then wiped dry with a damp cloth. Pre-weighed materials—sand, cement, mineral powder, and silica fume—were added sequentially into the mixer and blended for 180 s to achieve a homogeneous dry mix. Subsequently, two-thirds of the total mixing water, together with the superplasticizer, were added and mixed for 60 s, followed by the addition of the remaining water. Once the mixture exhibited suitable workability and viscosity, steel fibers were uniformly sieved into the mix through a 13 mm standard sample sieve. After this, mixing continued for an additional 480 s. The total mixing time was 13 min.

### *2.3 Curing Regime*

Following casting, both the RPC specimens (for material testing) and the composite deck model were promptly covered with plastic sheeting to minimize moisture loss. They were initially cured under controlled laboratory conditions—maintained at 20 ± 2°C and above 95% relative humidity—for the first 24 h. After demolding, the specimens were transferred to a standard curing room kept at 20 ± 2°C and >95% RH, where

they remained until reaching the designated testing age of 28 days. This normal-temperature wet-curing protocol was consistently applied to support the development of the RPC's mechanical properties without thermal treatment, in line with the study's emphasis on practicable field application.

### *2.4 Basic Mechanical Properties of RPC under Room Temperature Curing*

Preliminary laboratory experiments were performed to better understand the mechanical properties of RPC under normal-temperature curing. The mixing proportions for preparing the RPC sample are summarized in Table 1, and the RPC mixture was poured into designed molds to prepare three cube specimens with side length of 150 mm for the compression tests, six 150 mm × 150 mm × 300 mm cuboid specimens for the flexural strength tests, and three 100 mm × 100 mm × 400 mm cuboid specimens for the elastic modulus tests. After the modeled RPC specimens were cured at normal temperature to the required age, compression tests, flexural strength tests, and elastic modulus tests were performed separately. Fig. 1 shows an example of dynamic elastic modulus tests performed on a prepared cuboid specimen. Finally, the average value of compression strength, flexural strength, and elastic modulus of the RPC was obtained and summarized in Table 2. Table 2 shows that the compression strength, flexural strength, and elastic modulus of RPC under normal temperature curing have been obviously improved compared to those of the ordinary concrete in reference [19].

**Table 1:** Mixing ratio of the RPC specimens tested in this study.

| Material | Cement | Silica Sand | Silica Fume | Fly Ash | Quartz Powder | Water Reducer (%) | Steel Fibers by Volume (%) | Water to Cement Ratio |
|---|---|---|---|---|---|---|---|---|
| **Mixing ratio** | 1 | 1.1 | 0.2 | 0.1 | 0.2 | 2.5 | 3.7 | 0.21 |

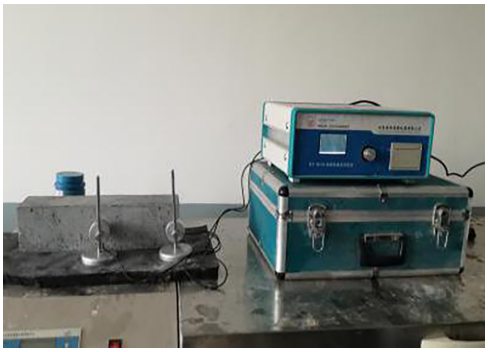

**Figure 1:** Dynamic elastic modulus test.

**Table 2:** Basic mechanical properties of RPC cured at room temperature.

| Cube Compression Strength (MPa) | Flexural Strength (MPa) | Elastic Modulus ($10^4$ MPa) | Unit Weight (kN/m$^3$) |
|---|---|---|---|
| 83.8 | 16.32 | 4.13 | 27 |

## 3 Stress Analysis of RPC Composite Deck

Using a bridge as the prototype, this study will establish local finite element models of one steel box girder and three types of composite box girders, followed by a comparative analysis. According to the literature [19], the dimensions of the local finite element models are as follows: the length of the bridge in the longitudinal direction is 0.8 m, the width of the bridge in the transverse direction was selected including six longitudinal stiffeners, that is 1.84 m, and the height is 0.214 m, of which the top plate is 14 mm thick, the diaphragm is 12 mm thick, the spacing of longitudinal rib is 300 mm, the longitudinal rib thickness 10 mm, the longitudinal rib height is 158 mm, the bottom plate width of longitudinal rib is 90 mm, and the diaphragm height is 200 mm.

### *3.1 Structural Details of Composite Bridge Decks*

The structural details of the three types of composite bridge decks are as follows:

1. Normal temperature RPC composite deck: 50 mm thick RPC layer under normal temperature curing was placed on the top of steel box girder bridge deck and connected using M20 shearing studs. The Poisson's ratio of RPC is 0.2 and the elastic modulus is 41,300 MPa.
2. High temperature RPC composite deck: 50 mm thick RPC layer under high temperature curing was placed on the top of steel box girder bridge deck and connected using M20 shearing studs. The Poisson's ratio of RPC is 0.2 [21] and the elastic modulus is 42,600 MPa.
3. Normal concrete composite deck: 50 mm thick normal concrete layer was placed on the top of steel box girder bridge deck and connected using M20 shearing studs. The weight is 25 kN/m$^3$, the Poisson's ratio of concrete is 0.24 [22] and the elastic modulus is 32,500 MPa.

The material parameters of the computational model are shown in Table 3.

**Table 3:** Table of material parameters.

| Parameters | Normal Temperature RPC | High Temperature RPC | Normal Concrete | Steel Box Girder |
|---|---|---|---|---|
| **Elastic Modulus (MPa)** | 41,300 | 42,600 | 32,500 | 210,000 |
| **Poisson's Ratio** | 0.2 | 0.2 | 0.24 | 0.3 |

### *3.2 Single-Span Local Model for Bridge Deck Calculation*

#### *3.2.1 Local Model Using Wheel Load*

It was assumed that the RPC was in continuous contact with the steel bridge deck. A local finite element model was established in ANSYS using SHELL63 elements for the steel box girder and SOLID65 elements for the concrete layers. To simulate the constraints from adjacent bridge segments, all degrees of freedom at the four vertical cut planes of the local model were fully constrained, a conventional approach for local stress analysis in orthotropic decks [21,25]. The interaction between the RPC/concrete layer and the steel deck was simulated using node coupling, assuming perfect bonding between the layers. A mapped meshing method was employed, with an element size determined through a mesh sensitivity analysis, to ensure convergence of the results. SHELL63 is an elastic shell element in ANSYS, suitable for modeling thin-plate structures. The orthotropic steel bridge deck is composed of welded thin steel plates (top plate, longitudinal ribs, and transverse diaphragms), whose thickness is significantly smaller than their planar dimensions, aligning with the fundamental assumptions of shell elements. Shell elements can effectively simulate the in-plane and out-of-plane mechanical behaviors of plates while offering high computational efficiency.

SOLID65 is a three-dimensional solid element developed in ANSYS based on SOLID45, specifically designed to account for the material properties of concrete-like materials. It can simulate nonlinear behaviors such as cracking and crushing. Although RPC (Reactive Powder Concrete) exhibits high strength, it still belongs to the category of concrete materials. Its mechanical behavior may involve three-dimensional stress states, making it suitable for simulation using solid elements. Furthermore, this element type allows for the inclusion of reinforcement bars or fiber-reinforced materials, making it applicable for RPC mixed with steel fibers.

In ANSYS, "node coupling" specifically refers to coupling the translational degrees of freedom of corresponding nodes at the interface between the RPC layer and the steel bridge deck. This enforces displacement compatibility between the two at the interface, simulating the rigid connection or strong bonding effect achieved in actual structures through shear studs—essentially assuming no relative slip between them. In the paper, based on the assumption of "fully continuous contact" between the RPC and the steel bridge deck, the node coupling method is employed to directly and thoroughly realize this connection condition. This approach avoids the uncertainty associated with intermediate contact states, facilitates the analysis of the overall stress distribution in the composite structure under load, and is particularly suitable for verifying the enhancing effect of the RPC layer on the mechanical performance of the steel bridge deck.

The specific dimensions of the local model are as follows: the longitudinal bridge direction length is 0.8 m, the transverse bridge direction covers the range of six stiffeners with a model width of 1.84 m, and the height is 0.214 m. Other dimensions are consistent with those of the background bridge. The local finite element model is shown in Fig. 2.

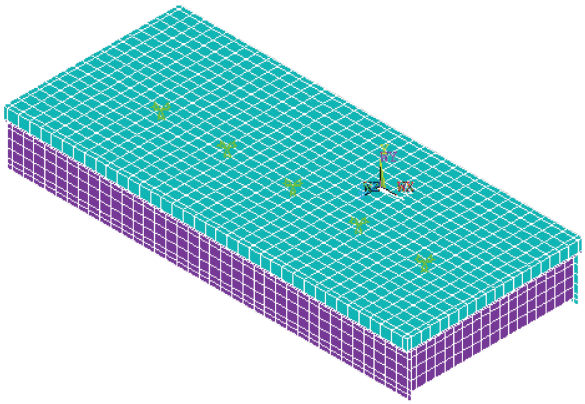

**Figure 2:** Local finite element model. (Local finite element model of the composite bridge deck segment established in ANSYS, showing the mesh configuration for the steel deck (using SHELL63 elements) and the RPC/concrete overlay (using SOLID65 elements). The model dimensions are 0.8 m (longitudinal) × 1.84 m (transverse) × 0.214 m (height), with boundary conditions simulating continuity to adjacent spans.).

Due to the presence of stiffeners in the longitudinal direction of the orthotropic steel plate, a negative bending moment will appear on the top surface of the stiffener during loading, and tensile stress will occur in the RPC layer. Therefore, the loading in the transverse direction is shown in Fig. 3, and the loading in the longitudinal direction was in the mid-span. Referring to the specifications of City Bridge Code, the vehicle load is a city A-class standard vehicle with the middle wheel weight of 100 kN, the applied load was 130 kN (the wheel weight 100 + 30% overload), and the local wheel load area size is 250 mm (longitudinal direction) × 600 mm (transverse direction).

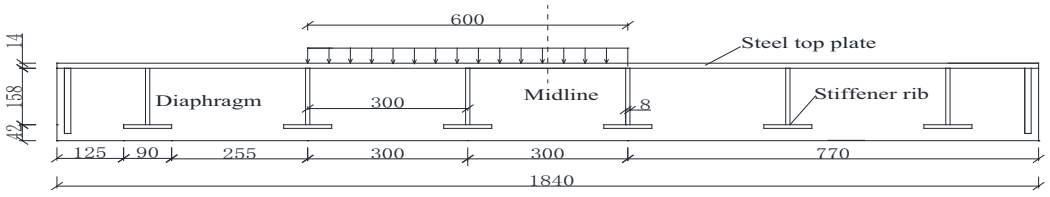


**Figure 3:** Loading model (Unit: mm).

### *3.2.2 Analytical Results Analysis*

In this study, stress data were recorded at three critical locations widely recognized as typical of fatigue. Prone hotspots in orthotropic steel decks [2,3]: (1) the top surface of the steel deck plate, midway between two longitudinal stiffeners (i.e., at the center of a deck plate panel); (2) the bottom flange of the longitudinal stiffener at the mid-span section; and (3) the bottom fibre of the RPC layer, located directly above the longitudinal stiffener—a key indicator for evaluating cracking and debonding resistance in RPC steel composite systems [11,13]. The calculated peak stresses of the steel bridge deck and the longitudinal stiffener are presented in Table 3; the calculated peak stress of the RPC layer is illustrated in Fig. 4.

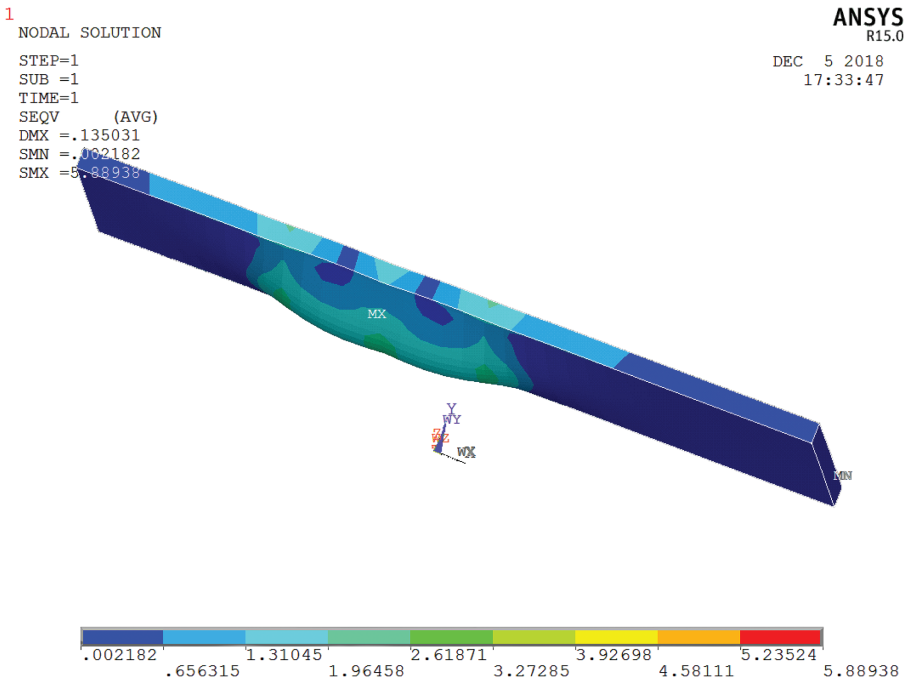


**Figure 4:** Stress contour plot of the RPC layer in the transverse direction under ambient curing.

It is shown in Table 4 that compared with the steel box girder, the stress is reduced with a maximum value of 91.03% and 87.74% in the transverse and longitudinal direction, respectively using the normal temperature RPC composite bridge deck; the stress is reduced with a maximum value of 91.43% and 88.22% in the transverse and longitudinal direction, respectively using the high temperature RPC composite bridge deck; and the stress is reduced with a maximum value of 87.63% and 84.34% in the transverse and longitudinal direction, respectively using the ordinary concrete composite bridge deck. It can be seen that the stress amplitude was significantly reduced using the three types of composite bridge deck. The literature [22]

mentions that the fatigue life is typically inversely proportional to the cube of the stress amplitude, so the fatigue life of the orthotropic steel bridge deck will be improved.

**Table 4:** Calculation results of peak stresses in orthotropic steel bridge deck.

| Location Stress | | Steel Box Girder | | Normal Temperature Cured RPC Composite Deck | | High Temperature Cured RPC Composite Deck | | Ordinary Concrete Composite Deck | |
|---|---|---|---|---|---|---|---|---|---|
| | | Tensile /MPa | Compressive /MPa | Tensile /MPa | Compressive /MPa | Tensile /MPa | Compressive /MPa | Tensile /MPa | Compressive /MPa |
| Steel deck | Transverse | 100.67 | −108.93 | 14.43 | −9.77 | 14.31 | −9.33 | 16.52 | −13.47 |
| | Longitudinal | 54.19 | −52.54 | 10.73 | −6.44 | 10.73 | −6.19 | 10.85 | −8.23 |

However, as shown in Table 5, the tensile stress in the transverse direction exceeds that in the longitudinal direction, and the transverse tensile stress surpasses the longitudinal tensile stress, with a maximum tensile stress of 1.720 MPa. The stress nephograms of the RPC layer in the transverse and longitudinal directions are shown in Figs. 4 and 5, respectively. Normal concrete is sufficient to withstand such stress levels.

**Table 5:** RPC layer stress peak results under normal temperature maintenance.

| Stress Direction | Tensile Stress/MPa | Compressive Stress/MPa |
|---|---|---|
| Longitudinal | 0.483 | −6.875 |
| Transverse | 1.720 | −5.472 |

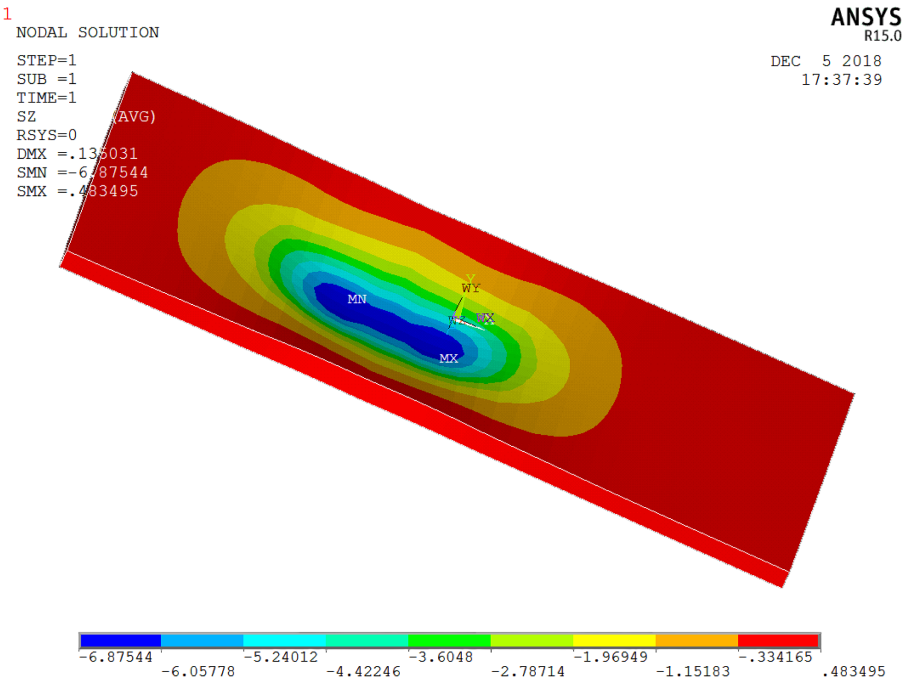


**Figure 5:** Longitudinal direction stress nephogram of the heat-cured RPC layer.

In order to show that the tensile strength of RPC is better than ordinary concrete, a two-span local model was established in this paper to analyze the composite bridge deck.

### *3.3 Two-Span Local Model for Bridge Deck Calculation*

#### *3.3.1 Local Model Using Wheel Load*

The longitudinal direction was selected to be 1.64 m. According to the principle of equivalent stress, the local model was designed as a 2 × 0.82 m two-span continuous beam. The vehicle load was applied using a Class A standard vehicle, as shown in Fig. 6. The other dimensions and the three composite bridge deck structures were identical to those of the single-span model. The loading included three positions in the longitudinal direction and two positions in the transverse direction, as shown in Fig. 7, where the loading position 3 is the wheel load of the No. 3 axis, and the loading positions 1 and 2 are the wheel combination loads of No. 1 and No. 2 axes. The load was considered to be 30% overloaded. By calculation, the most unfavorable load combination was the loading position 3 in the longitudinal direction and the loading position 2 in the transverse direction. The following calculations were based on the most unfavorable loading conditions.

#### *3.3.2 Analytical Results Analysis*

The calculated positions were consistent with the single-span model. The calculated peak stress of the two-span model (loading impact coefficient is set as 1.3) is shown in Table 5; the peak stress of the RPC layer is shown in Fig. 6.

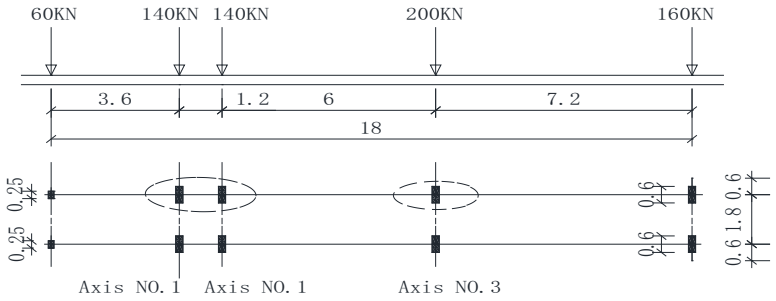


**Figure 6:** Arrangement of traffic loads.

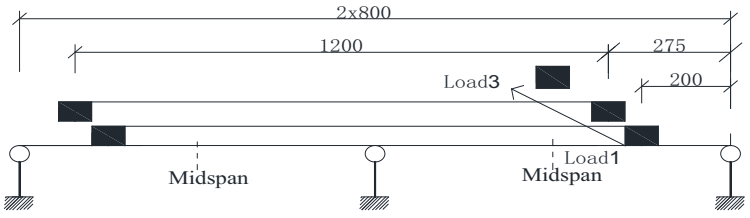


(**a**)

**Figure 7:** (Continued)

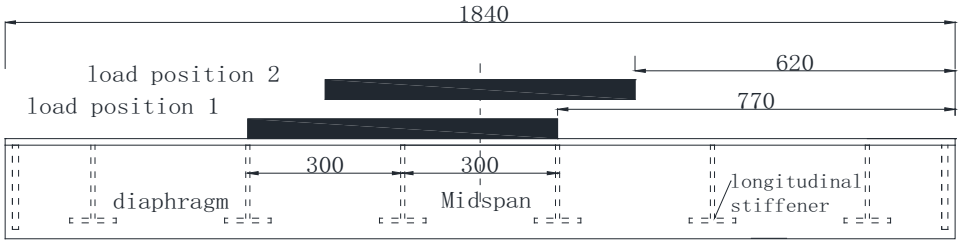


(**b**)

**Figure 7:** Loading position arrangement (**a**) in longitudinal direction; (**b**) in transverse direction.

Table 6 shows that compared with the steel box girder, the stress is reduced with a maximum value of 93.27% and 82.17% in the transverse and longitudinal direction, respectively using the normal temperature RPC composite bridge deck; the stress is reduced with a maximum value of 93.77% and 82.17% in the transverse and longitudinal direction, respectively using the high temperature RPC composite bridge deck; and the stress is reduced with a maximum value of 91.20% and 82.22% in the transverse and longitudinal direction, respectively using the ordinary concrete composite bridge deck. The maximum stress reduction of the normal temperature RPC composite bridge deck is 0.99 times that of the high temperature RPC composite deck, which is 1.02 times that of the ordinary concrete composite bridge deck. From the data analysis, the results of the two-span and single-span local model analyses are consistent, and the stress reduction difference between the normal temperature RPC composite bridge deck and the high-temperature RPC composite bridge deck is small.

**Table 6:** Calculation results of peak stresses in orthotropic steel bridge deck.

| Location Stress | | Steel Box Girder | | Normal Temperature Cured RPC Composite Deck | | High Temperature Cured RPC Composite Deck | | Ordinary Concrete Composite Deck | |
|---|---|---|---|---|---|---|---|---|---|
| | | Tensile /MPa | Compressive /MPa | Tensile /MPa | Compressive /MPa | Tensile /MPa | Compressive /MPa | Tensile /MPa | Compressive /MPa |
| Steel deck | Transverse | 215.82 | −212.40 | 18.19 | −14.28 | 17.90 | −13.22 | 21.44 | −18.68 |
| | Longitudinal | 72.19 | −91.29 | 14.57 | −16.28 | 14.54 | −16.27 | 16.47 | −16.23 |
| Longitudinal rib | Longitudinal | 120.70 | −183.79 | 86.81 | −129.52 | 85.93 | −128.15 | 89.89 | −134.41 |

Table 7 shows that the maximum tensile stress of the RPC layer in the normal temperature RPC composite bridge deck occurs in the longitudinal direction, with a value of 4.706 MPa. Fig. 8 shows the longitudinal stress nephogram of the RPC layer, from which it can be observed that the maximum tensile stress occurs above the central diaphragm. Therefore, ordinary concrete is unable to withstand this stress. This paper will verify if RPC experiences cracking under this stress by experimentation.

**Table 7:** RPC layer stress peak results under normal temperature maintenance.

| Stress Direction | Tensile Stress/MPa | Compressive Stress/MPa |
|---|---|---|
| Longitudinal | 4.706 | −8.264 |
| Transverse | 2.259 | −6.843 |

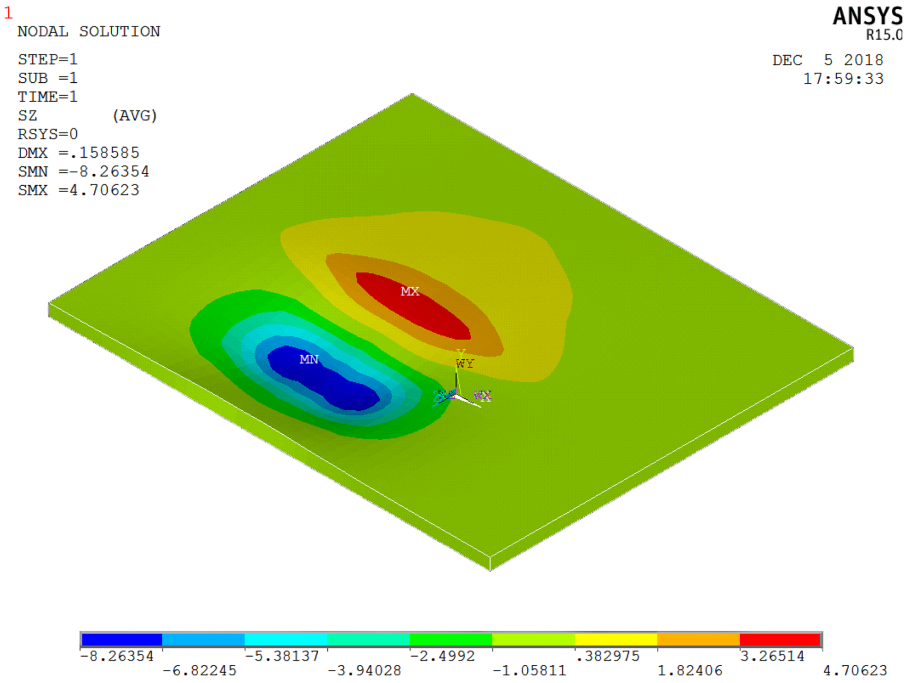


**Figure 8:** Longitudinal stress nephogram of RPC layer.

*3.3.3 Comparative Analysis of Deflection Results between Single-Span and Two-Span Local Models*

The deflection at mid-span Section 2 of the two-span local model is shown in Fig. 9a,b. The deflections of the steel-only deck, the normal concrete composite deck, the room-temperature cured RPC composite deck, and the heat-cured RPC composite deck are −0.649, −0.164, −0.153, and −0.150 mm, respectively. These results indicate that all three composite structures significantly enhance the stiffness of the bridge deck. However, the room-temperature cured RPC and heat-cured RPC composite decks demonstrate the most outstanding performance, which is consistent with the calculation results from the single-span local model. The deflection variation curve at the mid-span of the single-span model is shown in Fig. 10.

### *3.4 Local Model Test of Normal Temperature RPC Composite Bridge Deck*

*3.4.1 Local Model Tests Overview*

The size of the test specimen was the same as the finite element model of single-span model calculated above. Shear studs were welded on the steel deck and 50 mm thick RPC layer was cast afterwards.

Considering the stress in the transverse direction is relatively large, the transverse stress was used as the main control parameter. During construction, eight transverse stress gauges were placed on the RPC surface, and the positions are shown in Fig. 11.

The main test process involves the construction of steel box girder units, including the construction of shear studs, placement of strain gauges, and construction of reinforcing steel cages. This is followed by RPC layer pouring, room temperature curing, placement of strain gauges, and loading. Among them, the RPC was cured under normal temperature conditions (20 ± 3°C). It was watered twice daily and covered with a cloth to maintain humidity. The specimen was tested after 28 days, and no cracks appeared at the end of curing, as shown in Fig. 12a. The test set up is shown in Fig. 12b.

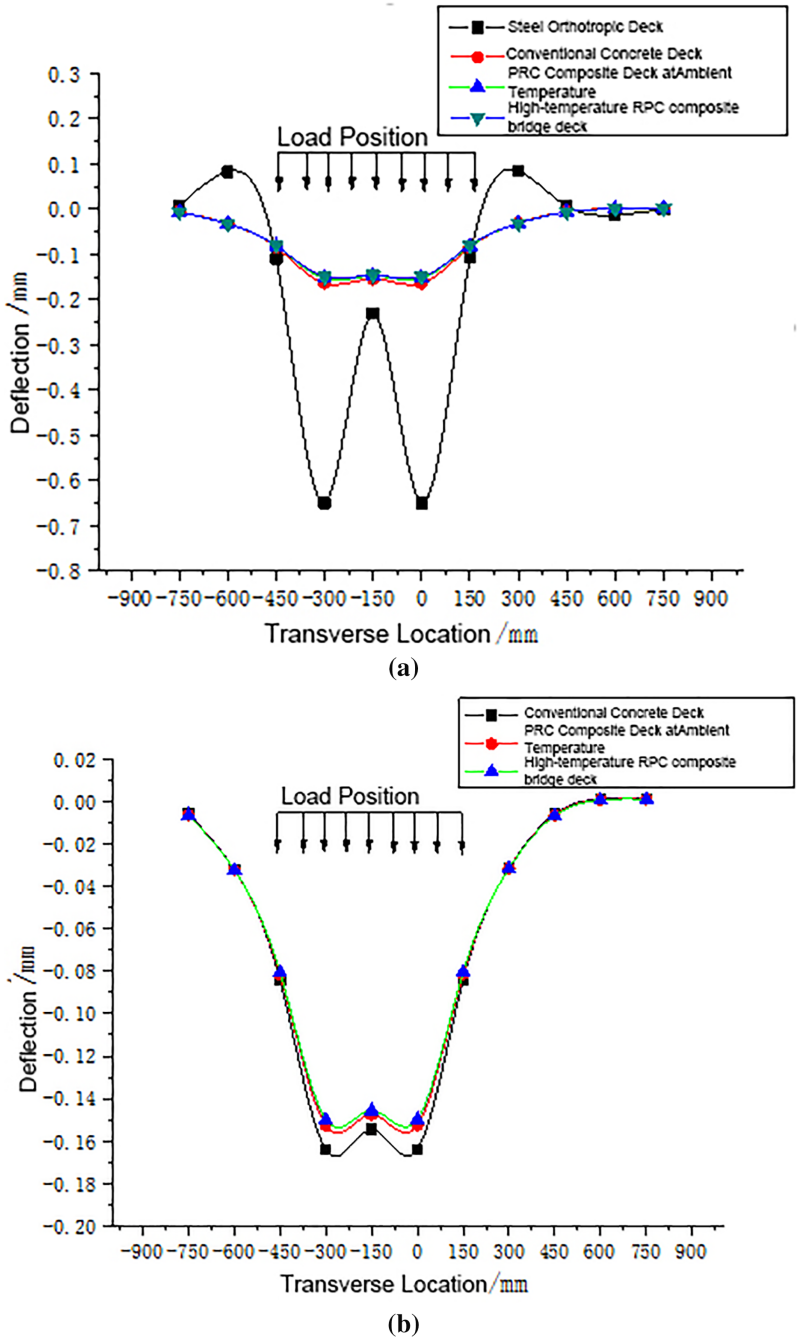


**Figure 9:** Deflection variation curve at mid-span section 2 of the two-span model. (**a**) deflection of mid-span section 2 for the four structures; (**b**) deflection of mid-span section 2 for the three structures.

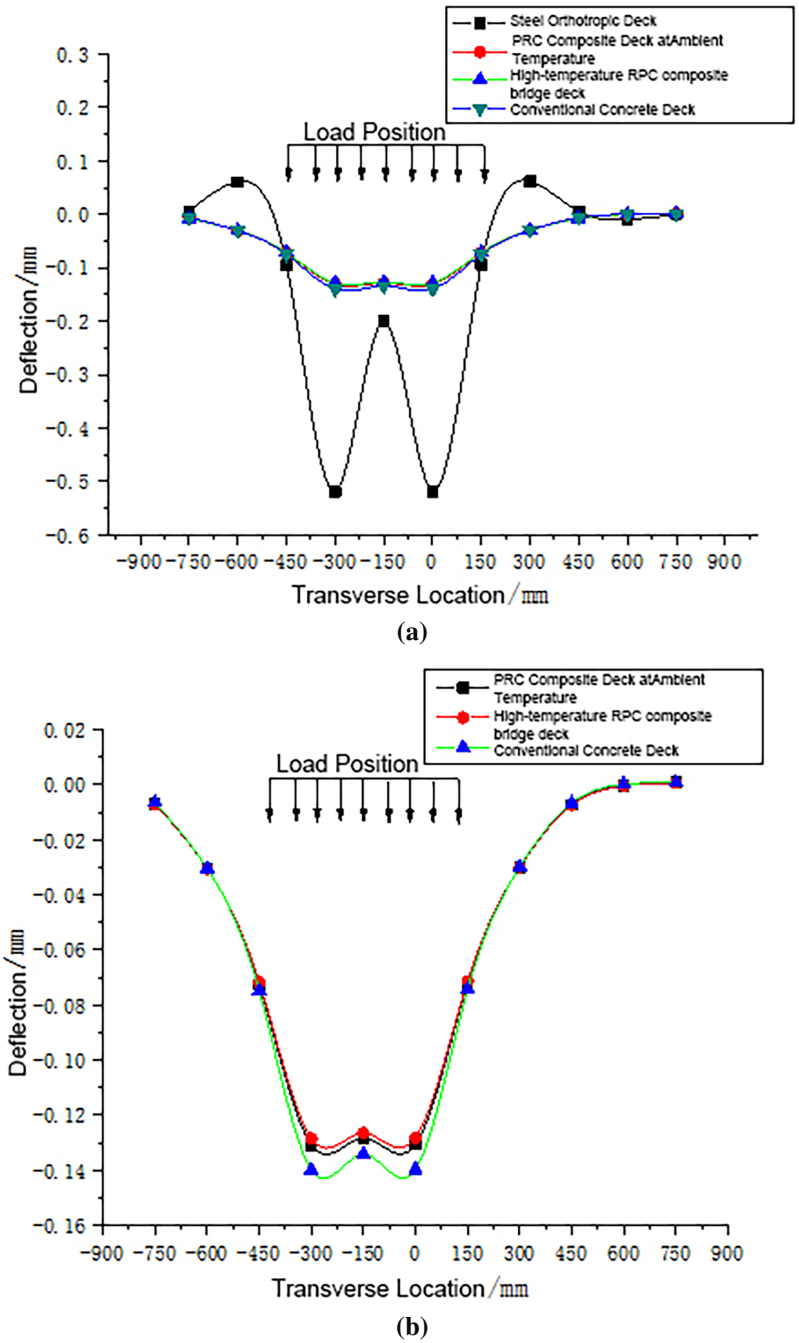


**Figure 10:** Deflection variation curve at mid-span of the single-span model. (**a**) deflection at mid-span for the four structural types; (**b**) deflection at mid-span for the three structural types.

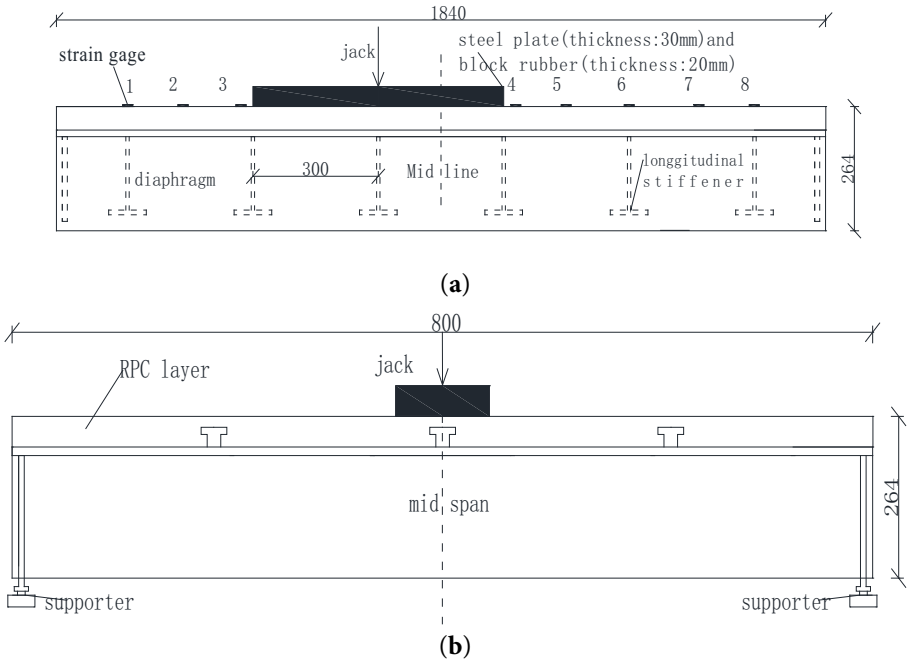


**Figure 11:** Test models. (**a**) in longitudinal direction; (**b**) in transverse direction.


**Figure 12:** (**a**) RPC surface after conservation; (**b**) Load test of model.

*3.4.2 Test Procedure*

The static load test was conducted following a systematic procedure to ensure data reliability:

Preparation and Pre-Loading: Prior to formal testing, a small pre-load (approximately 5% of the maximum load) was applied and removed three times to seat the specimen and stabilize the measurement system.

Loading Protocol: The load was then applied monotonically in discrete, sustained load steps. The designated load levels were 130, 250, and 350 kN, representing service, overload, and ultimate conditions, respectively.

Data Acquisition at Each Step: At each load level, the load was held constant for at least 5 min to allow for stress redistribution and to capture stable strain readings from all gauges (positions shown in Fig. 10). Strain data were recorded continuously using a digital data acquisition system at a sampling frequency of 1 Hz.

Visual Inspection: During and after each holding period, the RPC surface was thoroughly inspected for the initiation and propagation of any cracks.

Unloading: After reaching the maximum load (350 kN), the specimen was unloaded in reverse steps, and residual strains were recorded.

This stepwise procedure allowed for the clear correlation between load increment, structural response (strain and deflection), and observed damage state.

### *3.4.3 Primary Test Results*

The static loading test was performed at different levels. The transverse stress at the mid-span for a 130 kN loading level is shown in Table 8. A comparative analysis was subsequently performed against the ANSYS results. Fig. 13 illustrates the correlation between the experimental data and the numerical simulation results.

As shown in Table 8, the error at measuring point 4, located near the edge of the loading zone, is significantly larger than that at other locations. This discrepancy primarily arises from the severe stress concentration in this area, combined with the inevitable minor offset between the actual attachment position of the strain gauge (which was intentionally placed slightly away from the highest stress zone to avoid sensor damage during testing) and the corresponding calculation node in the finite element model. In regions with steep stress gradients, even a slight positional deviation can result in significant differences between measured and simulated values. In contrast, the errors at all other measuring points remain within 20%, showing consistent agreement with the ANSYS results and thereby verifying the overall rationality and accuracy of the finite element model. The elevated error at measuring point 4 is a localized phenomenon and does not undermine the core conclusion that the normal-temperature-cured RPC composite deck effectively reduces stress in the orthotropic steel deck and enhances its anti-cracking performance. This study acknowledges this localized deviation and suggests that future research and engineering applications could further improve measurement accuracy by optimizing the layout of measuring points—for instance, by avoiding zones with sharp stress variations or increasing the density of measurement points.

**Table 8:** RPC cross-bridge stress values at 130 kN.

| Test Point | RPC | | |
|---|---|---|---|
| | Test Value/MPa | ANSYS Value/MPa | Error/% |
| 1 | 1.038 | 0.881 | 15.12 |
| 2 | 1.341 | 1.111 | 17.15 |
| 3 | — | 0.939 | — |
| 4 | 1.433 | 0.916 | 36.08 |
| 5 | 1.408 | 1.133 | 19.53 |
| 6 | 1.227 | 1.007 | 17.93 |
| 7 | 0.429 | 0.374 | 12.82 |
| 8 | 0.061 | 0.055 | 9.83 |

Note: "—" indicates no value obtained.

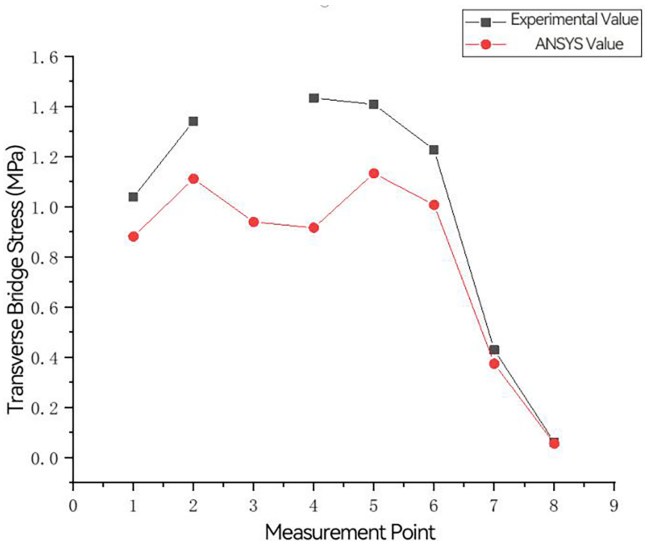


**Figure 13:** Comparison between Experimental and ANSYS Results (Comparison of transverse stress in the RPC layer between experimental measurements and ANSYS finite element predictions under a 130 kN wheel load at various gauge positions).

When the static load of 350 kN was applied, the stress value at measuring point 4 reached 1.37 times the maximum tensile stress (i.e., 4.706 MPa) of the RPC layer, as calculated by the finite element model of the normal temperature RPC composite box girder. No obvious cracks were observed in the RPC layer, which verified that the RPC's tensile strength is superior to that of ordinary concrete.

## 4 Discussion

This study demonstrates that the proposed normal-temperature-cured Reactive Powder Concrete (RPC) composite deck system provides a technically feasible and practically advantageous solution for orthotropic steel decks (OSDs).

### *4.1 Significant Stress Reduction and Fatigue Life Enhancement*

The finite element results (Table 3) indicate that both normal- and high-temperature-cured RPC overlays reduce the peak stress in the steel deck by over 90% compared to the pure steel deck, significantly outperforming the ordinary concrete overlay (approximately 87%–88% reduction). Crucially, the stress reduction achieved by the normal-temperature-cured RPC is virtually identical (within 1%) to that of its high-temperature-cured counterpart. This finding is of paramount importance, as it decouples the exceptional structural benefit of RPC from the energy-intensive and logistically challenging steam-curing process.

The implication of this stress reduction for fatigue performance is profound. According to classical fatigue theory, the fatigue life (N) of a metallic detail is inversely proportional to the cube of the applied stress range (S), i.e., $N \propto S^{-3}$ [20]. Applying this relationship, a 91.03% reduction in stress amplitude implies that the theoretical fatigue life at the critical deck plate location can be enhanced by a factor of approximately $(1/(1 - 0.9103))^3 \approx 1400$. Even for the ordinary concrete overlay with an 87.63% reduction, the life enhancement factor is about 60. This quantitative analysis highlights that the RPC overlay not only mitigates fatigue but can also fundamentally transform it from a dominant limit state into a remote concern, thereby significantly improving the durability and service life of OSDs.

### *4.2 Superior Crack Resistance and Material Performance*

A key experimental observation is the absence of cracking in the normal-temperature-cured RPC layer under a static load of 350 kN, corresponding to a calculated maximum tensile stress of 6.45 MPa. To contextualize this performance, the characteristic axial tensile strength of conventional C50 concrete is typically around 2.64 MPa. Therefore, the sustained stress in the RPC overlay is 2.4 times higher than the failure stress of ordinary concrete, unequivocally demonstrating its superior tensile capacity and crack resistance. This property directly addresses the historical weakness of rigid overlays, which often crack under their own tensile stresses [7,8]. The high fiber content (3.7% by volume) contributes to this enhanced post-cracking toughness and ductility, enabling the overlay to maintain integrity and continue providing composite action even under extreme loading.

### *4.3 Validation of the Numerical Model and Practical Implications*

The close agreement between the experimental strain readings (with errors largely within 20%) and the ANSYS predictions validates the developed finite element model. The localized larger error at measuring point 4 is attributed to stress concentration and minor placement offsets of the physical strain gauge, a known challenge in high-stress-gradient zones. The model's overall accuracy confirms its utility as a reliable tool for analyzing and designing such composite systems.

From a practical standpoint, the shift to normal-temperature curing is a critical innovation. It eliminates the need for site-based steam-curing facilities, simplifies the construction process, reduces energy consumption, and lowers costs. This makes the high-performance benefits of RPC accessible for a wider range of new construction and rehabilitation projects.

### *4.4 Contribution to Structural Resilience*

Beyond immediate mechanical improvements, this solution contributes to enhancing the resilience of bridge deck systems. Resilience, defined as the ability to withstand, adapt to, and recover from disturbances [24], is undermined by frequent repairs necessitated by pavement and fatigue damage. By simultaneously extending the fatigue life of the steel deck by orders of magnitude and providing a highly durable, crack-resistant wearing surface, the proposed system drastically reduces the frequency and urgency of maintenance interventions. This ensures longer periods of uninterrupted service, minimizes life-cycle costs, and improves the long-term sustainability and reliability of bridge infrastructure—core objectives of resilient engineering.

## 5 Conclusion

Based on the integrated numerical and experimental investigation, the following conclusions can be drawn:

1. Material Performance: Normal-temperature-cured RPC demonstrates superior mechanical properties compared to ordinary concrete, including a compressive strength of 83.8 MPa, a flexural strength of 16.32 MPa, and an elastic modulus of 41.3 GPa.
2. Structural Efficacy: The composite system incorporating a normal-temperature-cured RPC overlay reduces critical stresses in the orthotropic steel deck by more than 90%. This performance is statistically equivalent to that of a high-temperature-cured RPC overlay, yet it is achieved through a more practical and site-specific approach friendly curing process.

3. Fatigue and Crack Resistance: The substantial stress reduction implies a potential increase in fatigue life by several orders of magnitude. Moreover, the RPC overlay itself exhibits exceptional crack resistance, sustaining tensile stresses over twice the capacity of ordinary concrete without cracking.
4. Practical Application: This study confirms that the performance necessary to simultaneously mitigate pavement damage and steel deck fatigue is attainable without resorting to energy-intensive high-temperature curing. Consequently, the normal-temperature-cured RPC composite deck system offers a viable, efficient, and promising solution for improving the durability and structural resilience of orthotropic steel bridge decks in practice.

**Future Work:** Future research efforts should concentrate on three key areas: the long-term durability of the steel–RPC interface under cyclic fatigue loads; the structural performance under realistic traffic load spectra; and the formulation of standardized guidelines for the *in-situ* production and installation of normal-temperature-cured RPC overlays.

**Acknowledgement:** We would like to acknowledge the Lanzhou Jiaotong University Civil Engineering Laboratory for providing the raw materials essential for preparing the Reactive Powder Concrete (RPC) in this study. We also wish to thank Grammarly (www.grammarly.com) for its assistance in grammar checking and language polishing during the manuscript preparation.

**Funding Statement:** This research was supported by the following funding sources: The National Natural Science Foundation of China (Grant Numbers 51508255 and 51669010). The Natural Science Foundation of Gansu Province, China (Grant Numbers 17JR5RA105 and 1506RJZA082). The Gansu Provincial Joint Foundation (Grant Numbers 24JRRA799, 24JRRA857 and 25JRRA1119). The funders had no role in the design of the study; in the collection, analyses, or interpretation of data; in the writing of the manuscript; or in the decision to publish the results.

**Author Contributions:** Hui Zhang: Conceptualization, Methodology, Funding acquisition, Supervision, Writing—review & editing. Yingying Xie: Investigation, Formal analysis, Data curation, Writing—original draft. Yu Zhang: Resources, Validation, Writing—review & editing. Zhan Gao: Software, Validation, Visualization. Aijun Li, Sheng Shi: Investigation, Resources. Xingyue Li, Zheming Zhou, Haotian Wang: Formal analysis, Data curation. All authors reviewed and approved the final version of the manuscript.

**Availability of Data and Materials:** The large-scale raw datasets generated during this study (e.g., high-resolution strain field images, detailed FE output files) are not deposited in a public online repository due to their substantial volume and specialized formats. However, they are available from the corresponding authors upon reasonable request via offline storage media (e.g., hard drive).

**Ethics Approval:** This study did not involve human participants, animal experiments, or any other procedures requiring ethical approval. Therefore, ethics approval was not required.

**Conflicts of Interest:** The authors declare no conflicts of interest.

## References

1. Pipinato A. Innovative bridge design handbook: construction, rehabilitation and maintenance. 2nd ed. Amsterdam, The Netherlands: Butterworth-Heinemann; 2021. p. 711–27.
2. Qian ZH, Abruzzese D. Fatigue failure of welded connections at orthotropic bridges. Frat Ed Integrità Strutt. 2009;3(9):105–12. doi:10.3221/igf-esis.09.11.
3. Wang CS, Fu BN, Zhang Q, Feng YC. Fatigue test on full-scale orthotropic steel bridge deck. China J Highw Transp. 2013;26(2):69–76. (In Chinese). doi:10.2208/jscej.1989.410_25.
4. Ke L, Li C, He J, Lu Y, Jiao Y, Liu Y. Fatigue evaluation and CFRP strengthening of diaphragm cutouts in orthotropic steel decks. Steel Compos Struct. 2021;39(4):453–69. doi:10.4028/www.scientific.net/amr.1025-1026.17.

5. Walter R, Olesen JF, Stang H, Vejrum T. Analysis of an orthotropic deck stiffened with a cement-based overlay. J Bridge Eng. 2007;12(3):350–63. doi:10.1061/(asce)1084-0702(2007)12:3(350).
6. Gaul R. A long life pavement for orthotropic bridge decks in China. In: Proceedings of the 2009 GeoHuan International Conference, Challenges and Recent Advances in Pavement Technologies and Transportation Geotechnics; 2009 Aug 3–6; Changsha, China. p. 1–8.
7. Panichev A, Usoltsev A, Ivanov A, Poljakov S. Increasing the durability of pavement on operational steel spans by reinforcement with composite materials. Transp Res Procedia. 2022;63(1):1927–35. doi:10.1016/j.trpro.2022.06.213.
8. Feng Q, Zhu Z, Tong Q, Yu Y, Zheng W. Dynamic responses and fatigue assessment of OSD in heavy-haul railway bridges. J Constr Steel Res. 2023;204:107873. doi:10.1016/j.jcsr.2023.107873.
9. Liu Y, Shen Z, Liu J, Chen S, Wang J, Wang X. Advances in the application and research of steel bridge deck pavement. Structures. 2022;45(4):1156–74. doi:10.1016/j.istruc.2022.09.084.
10. Yao ZX. Study on mechanical properties and fatigue life of reactive powder concrete. J Railw Sci Eng. 2016;13(7):1275–81. (In Chinese). doi:10.19713/j.cnki.43-1423/u.2016.07.008.
11. Shao X, Yi D, Huang Z, Zhao H, Chen B, Liu M. Basic performance of the composite deck system composed of orthotropic steel deck and ultrathin RPC layer. J Bridge Eng. 2013;18(5):417–28. doi:10.1061/(asce)be.1943-5592.0000348.
12. Shao X, Qu W, Cao J, Yao Y. Static and fatigue properties of the steel-UHPC lightweight composite bridge deck with large U ribs. J Constr Steel Res. 2018;148:491–507. doi:10.1016/j.jcsr.2018.05.011.
13. Li J, Feng XT, Shao XD, Wang Y, Cao JH. Comparison of mechanical calculation and actual test for new STC steel bridge paving system. China J Highw Transp. 2014;27(3):39–44,50. (In Chinese). doi:10.19721/j.cnki.1001-7372.2014.03.006.
14. Xue J, Briseghella B, Huang F, Nuti C, Tabatabai H, Chen B. Review of ultra-high performance concrete and its application in bridge engineering. Constr Build Mater. 2020;260:119844. doi:10.1016/j.conbuildmat.2020.119844.
15. He F, Huang ZY. Selection of raw materials and parameters of mix design for active powder concrete. New Build Mater. 2007;34(3):74–7. (In Chinese). doi:10.3969/j.issn.1001-702X.2007.03.022.
16. Deng M, Huo N, Shi G, Zhang J. Shear strength analysis of the stud in steel-UHPC composite bridge deck. IOP Conf Ser Earth Environ Sci. 2017;100(1):012176. doi:10.1088/1755-1315/100/1/012176.
17. Du G, Bu L, Yang D. Experimental study and numerical simulation on the flexural performance of section steel beams strengthened by wrapping reinforced RPC under secondary load. Eng Struct. 2022;270(1):114816. doi:10.1016/j.engstruct.2022.114816.
18. Wang WQ. The research on key technologies of assembled light composite deck system composed of steel deck and RPC [master's thesis]. Changsha, China: Hunan University; 2010.
19. Zhang H, DesRoches R, Yang Z, Liu S. Experimental and analytical studies on a streamlined steel box girder. J Constr Steel Res. 2010;66(7):906–14. doi:10.1016/j.jcsr.2010.02.001.
20. Shao XD, Zhang Z, Liu ML, Cao JH. Research on bending tensile strength for composite bridge deck system composed of orthotropic steel deck and thin RPC topping. J Hunan Univ Nat Sci. 2012;39(10):7–13. (In Chinese). doi:10.3969/j.issn.1674-2974.2012.10.002.
21. Liu S, Ji W, Mao Y, Li L, Zhang X. Finite element analysis and test research on fish-bellied steel box beam with orthotropic deck and composite pavement. China Civ Eng J. 2011;44(S1):128–34. doi:10.4028/www.scientific.net/amm.275-277.1163.
22. Shao XD, Cao JH, Yi DT, Chen B, Huang ZY. Research on basic performance of composite bridge deck system with orthotropic steel deck and thin RPC layer. China J Highw Transp. 2012;25(2):40–5. (In Chinese). doi:10.1061/(asce)be.1943-5592.0000348.
23. Bai Q, Xin Z, Ma HY, Sun WH, Liu HB, Jiang CJ. Graphite tailings powder driving the low-carbon transformation of ultra-high performance concrete (UHPC): innovative pathways for solid waste resource utilization and synergistic mechanisms for performance enhancement. Constr Build Mater. 2025;486:141932. doi:10.1016/j.conbuildmat.2025.141932.
24. Forcellini D, Kalfas KN. A framework to quantify the impact of deterioration on the seismic resilience of structures. Struct Infrastruct Eng. 2025:1–9. doi:10.1080/15732479.2025.2591824.

25. Yuan Z, Jia Y, Sun J, Zhang X, Hu Y, Han X. Study on the properties of high fly ash content alkali-activated fly ash slag pastes and fiber-reinforced mortar under normal temperature curing. Materials. 2024;17(22):5668. doi:10.3390/ma17225668.
26. Xu C, Xiao H, Wang W, Ma B, Cheng B, Su Q. Thermostatic shrinkage effect monitoring and analysis of novel post-combination steel-UHPC composite decks. Eng Struct. 2023;295:116864. doi:10.1016/j.engstruct.2023.116864.
27. Liu Y, Bao Y, Deng L, Zhang Q. Numerical study on the effects of stud degradation and stud arrangement on the fatigue performance of steel-UHPC composite decks. Eng Struct. 2023;292:116549. doi:10.1016/j.engstruct.2023.116549.
28. Huang Y, Chen S, Gu P. Interface stress analysis and fatigue design method of steel-ultra high performance concrete composite bridge deck. Structures. 2022;38:1453–64. doi:10.1016/j.istruc.2022.03.005.
29. Yuan Y, Wu C, Jiang X. Experimental study on the fatigue behavior of the orthotropic steel deck rehabilitated by UHPC overlay. J Constr Steel Res. 2019;157:1–9. doi:10.1016/j.jcsr.2019.02.010.
30. Di J, Ruan X, Zhou X, Wang J, Peng X. Fatigue assessment of orthotropic steel bridge decks based on strain monitoring data. Eng Struct. 2021;228:111437. doi:10.1016/j.engstruct.2020.111437.